

A catalog of planetary nebulae in the elliptical galaxy NGC 4697¹

R. H. Méndez, A. M. Teodorescu, and R.-P. Kudritzki

Institute for Astronomy, University of Hawaii, 2680 Woodlawn Drive, Honolulu, HI 96822

mendez@ifa.hawaii.edu

ABSTRACT

We present a catalog of 535 planetary nebulae discovered in the flattened elliptical galaxy NGC 4697, using the FORS1 Cassegrain spectrograph of the Very Large Telescope of the European Southern Observatory at Cerro Paranal, Chile. The catalog provides positions (x, y coordinates relative to the center of light of NGC 4697, as well as α, δ), and, for almost all PNs, the magnitude $m(5007)$ and the heliocentric radial velocity in km s^{-1} .

Subject headings: galaxies: elliptical and lenticular, cD — galaxies: individual (NGC 4697) — galaxies: kinematics and dynamics — planetary nebulae: general

1. Introduction

We present a catalog of 535 planetary nebulae (PNs) discovered in the flattened elliptical galaxy NGC 4697, using the FORS1 Cassegrain spectrograph of the Very Large Telescope of the European Southern Observatory at Cerro Paranal, Chile. The observations and scientific results have been described in Méndez et al. (2001, in what follows Paper I). The interpretation of the most important result, which can be described as a Keplerian decline of line-of-sight velocity dispersion as a function of angular distance from the center of the galaxy, has been quite difficult. Several theoretical groups are working on the development of better numerical models, including three-integral models better adapted to a flattened dynamical system like NGC 4697. We have decided to publish the catalog now, so as to make it available to all interested groups. We have recalculated the radial velocities in one of the observed fields, using a different procedure than the one described in Paper I. After confirming that no important changes were necessary, we have combined the two sets of measurements into one final catalog. The catalog provides positions (x, y coordinates relative

¹The data presented herein were obtained at the European Southern observatory, Cerro Paranal, Chile, Program ESO 63.I-0008.

to the center of light of NGC 4697, as well as α, δ), and, for almost all PNs, the magnitude $m(5007)$ and the heliocentric radial velocity in km s^{-1} .

We also provide a list of peculiar, mostly emission-line objects that are not planetary nebulae, for eventual future studies. In section 2 we describe the radial velocity recalculations mentioned above, and compare the new versus the old velocities. Section 3 contains the catalog, and Section 4 is devoted to the peculiar objects we detected.

2. Radial velocity recalculations

Planetary nebulae in NGC 4697 were discovered using a combination of onband images, offband images, and onband + grism dispersed images. For details, please refer to Paper I (Méndez et al. 2001).

In Paper I, the registration of grism images was performed using the dispersed images of stars. This introduces a problem, already described in Paper I, Section 3: since the on-band filter transmission curve shifts in wavelength as a function of ambient temperature, it turns out that the positions of the spectral segments of continuum sources in the grism images are dependent on temperature, while the positions of emission-line sources are not affected. One of the two fields observed in Paper I, namely field W, was obtained by combining images taken in two different years at somewhat different temperatures; since the temperature-dependent positions of dispersed stars were used for the registration, the PN positions in different years were slightly different.

Although this problem could be detected and corrected, using the positions of bright PNs in the individual reference image for field W, we always wanted to redo the registration for this field using directly the brightest PNs visible in all the individual images, instead of using the dispersed star segments, because, using the PNs, the temperature effect is completely avoided. We have finally done so. For the new registration we used 30 bright PNs visible in the individual W onband exposures. Once the new combined W dispersed image was produced, we remeasured the positions of all PNs previously detected in the W field, and recalculated all their radial velocities. Fig. 1 shows the comparison of old versus new velocities for all PNs in the W field. Fig. 2 shows the difference between new and old W velocities as a function of the new W velocities. The agreement is satisfactory, but there is a small systematic difference of about 20 km s^{-1} . This offset is also visible in Figs. 3 and 4, where the differences are plotted respectively as a function of the $m(5007)$ magnitudes, and of the E velocities (where available). Note in Fig. 3 how the differences get larger for fainter PNs, as expected, since the quality of the radial velocities depends on the quality of

the position measurements.

The systematic difference between old and new W velocities is unexpected, because the new measurements are not supposed to be less reliable than the old ones. We have not found an explanation for the offset. We could have ignored the new measurements and kept the old ones, but we feel it is more honest to consider old and new W measurements as independent (because a new combined image was generated and measured) and equally valid. Consequently, and since the offset is small in comparison to errors of about 40 km s^{-1} , as estimated in Paper I, we decided to average the two radial velocities for each PN in the W field. The resulting W radial velocities were then averaged with the corresponding velocities from detections in the E field, when available.

Fig. 5 shows the velocities of 531 PNs as a function of their x -coordinates relative to the center of NGC 4697; this is essentially the same as Figure 20 in Paper I, confirming that there is no significant change in the radial velocity distribution. In other words, all discussions and conclusions in Paper I remain valid.

3. The PN catalog

In Table 1 we list the following: identification numbers for both E and W fields; (x, y) coordinates, in pixels, relative to the optical center of NGC 4697; J2000 equatorial coordinates; Jacoby magnitudes $m(5007)$; and heliocentric radial velocity in km s^{-1} .

It may be useful to point out that the identification numbers do not follow a continuous sequence; they were assigned in arbitrary order as the PNs were being discovered, and the numbers for objects in field W start at 1001 in order to avoid any confusion with E field numbers, which are all below 1000. A few numbers are missing because the corresponding objects were rejected as PNs. There is also a discontinuity between W1217 and W1501. We prefer to keep these original identification numbers unchanged, for our own reference in future studies and because some of these numbers have already been used in another publication, namely the chemical abundance study (Méndez et al. 2005). An identification number -1 was assigned in Table 1 to objects not present in the corresponding field.

The original on-band and off-band images (fields E and W) were oriented with the x -axis in the direction of the major axis. The combined images are available in fits format upon request. We have not listed the PN pixel coordinates in each combined on-band image, because they can be easily obtained from the (x, y) values in the catalog, knowing that the (x, y) pixel coordinates of the center of NGC 4697 in the E and W images are, respectively, (1543, 979) and (373, 968).

The J2000 equatorial coordinates were calculated using a set of astrometric programs written by David Tholen and kindly provided by Fabrizio Bernardi. A first program, when given an input file with field and camera parameters, identifies all the USNO-B1 catalog stars available within the desired field and produces a list of reference stars with rough estimates of their position in the chip. The next programs make an improved centroid fitting for reference stars, producing an output file with a list of reference stars with pixel coordinates x, y accurate to a few hundredths of a pixel. The last program performs the final astrometric fit, rejecting outliers and iterating, and provides the PN equatorial coordinates with uncertainties of about 0.2 arcsecond. We list those final equatorial coordinates in Table 1. The uncertainty in RA and declination close to the center of NGC 4697 is probably a bit larger, about 0.5 arcsecond, because there are almost no reference stars near that position.

The definition of Jacoby magnitudes $m(5007)$ can be found in Paper I, Section 4. Or see Jacoby (1989). Typical uncertainties for these magnitudes are 0.1 and 0.2 mag for PNs brighter and fainter than $m(5007) = 26.5$, respectively.

Finally, in Paper I we estimated that the heliocentric radial velocities have uncertainties of about 35 or 40 km s⁻¹. For both magnitudes and heliocentric radial velocities, a value of -1 in Table 1 indicates that the corresponding quantity could not be measured.

4. A list of other sources in the field of NGC 4697

The PN search method, based on taking onband, offband and (onband+grism) images, is affected by some contamination from other sources. Since some of these might become interesting for other purposes, we have decided to list them. These objects can be assigned to one or another of the following groups:

(1) Emission-line regions within an extended source, presumably star-forming galaxies at such redshifts that some emission line falls into the on-band filter transmission curve (e.g. [O II] $\lambda 3727$ at $z = 0.35$).

(2) Point sources visible not only in the onband and grism images, but also in the offband image. These could be high-redshift quasars or star-forming regions (e.g. showing Lyman α redshifted into the onband filter at $z = 3.1$), or perhaps even a PN within a globular cluster that belongs to NGC 4697 (one such globular cluster was reported in NGC 5128 by Minniti and Rejkuba 2002). The object is rejected as a PN because it is visible in the offband image; but of course it would have to be reaccepted as PN if the last interpretation were to be confirmed.

(3) Point sources visible in the onband and grism images, and invisible in the offband image, but having a radial velocity incompatible with NGC 4697 if the emission line is assumed to be [O III] $\lambda 5007$. Three such sources were reported in Paper I, and we include them here.

(4) Sources stronger in the offband image, presumably star-forming galaxies or quasars with some emission line redshifted into the offband filter.

(5) A few sources were found to be stronger in the onband image than in the offband image, but no emission line was detectable in the grism image. Perhaps these are variable stars.

Table 2 lists a total of 20 sources, providing the x, y pixel coordinates relative to the center of NGC 4697, the J2000 equatorial coordinates, and a brief description. A search within the Simbad reference database has not produced any coincidence of objects in Table 2 with known sources. Object 10 in Table 2 is very close (a few arcseconds) to object 29 in the list of Chandra X-ray sources of Sarazin, Irwin, & Bregman (2001), but given the small coordinate uncertainties we believe these two sources are not related.

The work presented here has been supported by the National Science Foundation under Grant No. 0307489. We would like to thank Fabrizio Bernardi for his help using David Tholen’s astrometric programs for the calculation of J2000 equatorial coordinates.

REFERENCES

- Jacoby, G.H. 1989, ApJ, 339, 39
- Méndez, R.H., Riffeser, A., Kudritzki, R.P., et al. 2001, ApJ, 563, 135
- Méndez, R.H., Thomas, D., Saglia, R.P., et al. 2005, ApJ, 627, 767
- Minniti, D., & Rejkuba, M. 2002, ApJ, 575, L59
- Sarazin, C.L., Irwin, J.A., & Bregman, J.N. 2001, ApJ, 556, 533

Table 1. Planetary nebulae in NGC 4697 ^a

Id, E	Id, W	x , G	y , G	α	(2000)	δ	(2000)	$m(5007)$	Helioc. RV
7	1001	-295	-801	12	48	44.02	-5 50	26.6	1228
9	1070	41	-894	12	48	40.47	-5 50	26.9	980
20	1002	-254	-670	12	48	42.78	-5 49	27.3	1354
21	1004	-209	-581	12	48	41.73	-5 49	26.3	1283
22	1003	-181	-713	12	48	42.14	-5 49	27.4	1283
23	1071	-110	-707	12	48	41.25	-5 50	27.4	1140
24	1072	-90	-667	12	48	40.78	-5 49	26.5	1266
25	1073	38	-596	12	48	38.82	-5 49	26.1	995
45	1005	-254	-554	12	48	42.14	-5 49	26.7	1120
46	1006	-255	-460	12	48	41.61	-5 49	25.9	1406
47	1007	-181	-457	12	48	40.70	-5 49	26.4	1063
48	1008	-169	-391	12	48	40.17	-5 48	27.7	1006
49	1074	-100	-479	12	48	39.84	-5 49	26.8	1244
50	1075	-62	-429	12	48	39.09	-5 49	26.7	1492
51	1076	-54	-437	12	48	39.04	-5 49	26.7	1463
53	1078	-52	-378	12	48	38.69	-5 49	26.2	1033
54	1079	23	-413	12	48	37.98	-5 49	26.1	1060
55	1080	-29	-477	12	48	38.97	-5 49	27.9	1320
56	1081	0	-509	12	48	38.79	-5 49	27.3	1275
57	1082	35	-517	12	48	38.40	-5 49	27.6	1407
61	1157	101	-510	12	48	37.58	-5 49	27.5	1422
62	1158	103	-520	12	48	37.60	-5 49	26.6	1124
86	1010	-329	-326	12	48	41.76	-5 48	26.5	1030
87	1009	-311	-360	12	48	41.72	-5 48	27.5	1377
88	1017	-275	-243	12	48	40.62	-5 48	27.2	1232
89	1016	-262	-209	12	48	40.26	-5 48	26.9	1254
90	1011	-259	-297	12	48	40.74	-5 48	26.7	1598
91	1018	-193	-277	12	48	39.82	-5 48	27.7	1399
92	1014	-195	-225	12	48	39.55	-5 48	26.6	1452
93	1015	-183	-207	12	48	39.29	-5 48	26.9	1472
94	1019	-158	-271	12	48	39.36	-5 48	27.7	1355
95	1012	-160	-261	12	48	39.33	-5 48	27.1	1352
96	1013	-160	-253	12	48	39.29	-5 48	26.7	1119
97	1023	-159	-220	12	48	39.09	-5 48	28.0	1553
98	1083	-144	-177	12	48	38.66	-5 48	22.1	1427
99	1084	-121	-176	12	48	38.38	-5 48	23.9	1464
100	1085	-98	-168	12	48	38.05	-5 48	24.5	1298
101	1086	-48	-172	12	48	37.47	-5 48	29.2	789
102	1087	40	-173	12	48	36.40	-5 48	37.0	1271
103	1162	67	-164	12	48	36.02	-5 48	37.8	1464
104	1088	-69	-214	12	48	37.97	-5 48	35.2	1416
105	1089	-29	-197	12	48	37.38	-5 48	35.6	1487
106	1090	34	-205	12	48	36.65	-5 48	42.3	920
107	1091	24	-269	12	48	37.14	-5 48	53.1	1242
108	1163	61	-291	12	48	36.82	-5 49	0.2	1223
109	1092	-104	-320	12	48	38.99	-5 48	51.5	1286
110	1093	-92	-343	12	48	38.97	-5 48	56.6	1121
111	1094	-39	-324	12	48	38.23	-5 48	57.8	1455
112	1095	-37	-337	12	48	38.27	-5 49	0.2	1345
136	1024	-333	-26	12	48	40.09	-5 47	38.9	1148
143	1025	-251	35	12	48	38.76	-5 47	34.7	1364
144	1026	-179	33	12	48	37.90	-5 47	41.2	1094
145	1027	-167	26	12	48	37.79	-5 47	43.5	975
146	1097	-132	34	12	48	37.32	-5 47	45.0	1153
147	1028	-273	14	12	48	39.14	-5 47	36.8	1006
148	1029	-271	-0	12	48	39.20	-5 47	39.4	1015
149	1030	-253	10	12	48	38.92	-5 47	39.2	1054
150	1031	-237	19	12	48	38.67	-5 47	38.8	1297
151	1032	-212	9	12	48	38.43	-5 47	42.7	1082
153	1034	-181	10	12	48	38.05	-5 47	45.3	1117
155	1036	-302	-23	12	48	39.69	-5 47	40.9	1321
156	1037	-259	-21	12	48	39.17	-5 47	44.3	983
157	1038	-252	-41	12	48	39.20	-5 47	48.4	1026
158	1039	-230	-55	12	48	39.02	-5 47	52.8	1300
159	1040	-261	-67	12	48	39.45	-5 47	52.3	1135
160	1041	-248	-68	12	48	39.30	-5 47	53.7	1491
161	1042	-309	-66	12	48	40.03	-5 47	48.1	1120

Table 1—Continued

Id, E	Id, W	x , G	y , G	α	(2000)	δ	(2000)	$m(5007)$	Helioc. RV	
162	1043	-301	-69	12	48	39.96	-5 47	49.4	26.4	1226
163	1044	-287	-105	12	48	39.99	-5 47	57.0	27.0	1174
164	1020	-272	-157	12	48	40.10	-5 48	7.8	27.2	1253
165	1045	-240	-131	12	48	39.57	-5 48	5.7	26.6	1040
166	1022	-228	-145	12	48	39.50	-5 48	9.3	26.4	1234
167	1021	-172	-149	12	48	38.84	-5 48	14.8	26.9	1252
168	1098	-134	-65	12	48	37.91	-5 48	2.8	27.0	906
169	1099	-112	26	12	48	37.12	-5 47	48.1	25.7	1410
170	1100	-87	26	12	48	36.81	-5 47	50.2	25.8	1418
171	1101	-105	-4	12	48	37.19	-5 47	54.2	25.9	1481
172	1102	-120	-46	12	48	37.62	-5 48	0.5	25.9	1126
173	1103	-114	-40	12	48	37.51	-5 47	59.9	26.6	1116
174	1104	-104	-121	12	48	37.86	-5 48	15.4	26.3	1140
175	1105	-76	-99	12	48	37.39	-5 48	13.8	26.8	1171
176	1106	-73	-107	12	48	37.40	-5 48	15.4	26.5	1210
177	1107	-58	-137	12	48	37.39	-5 48	22.3	26.6	1214
178	1108	-24	-60	12	48	36.54	-5 48	11.2	26.2	1242
179	1109	-9	-82	12	48	36.49	-5 48	16.4	26.2	1434
180	1110	-4	-135	12	48	36.72	-5 48	26.4	26.5	1065
181	1096	11	-161	12	48	36.68	-5 48	32.5	27.1	1159
182	1111	42	-115	12	48	36.06	-5 48	26.7	26.5	1136
183	1165	62	-91	12	48	35.67	-5 48	24.0	26.8	1228
184	1112	32	-46	12	48	35.79	-5 48	13.4	26.9	1576
185	1166	89	17	12	48	34.73	-5 48	6.8	26.3	1231
186	1167	97	12	12	48	34.66	-5 48	8.3	25.9	1346
200	1180	91	-39	12	48	35.02	-5 48	17.1	25.8	1642
203	1183	76	-85	12	48	35.47	-5 48	24.2	26.4	1170
204	1184	91	-91	12	48	35.32	-5 48	26.4	26.2	1325
205	1185	93	-121	12	48	35.46	-5 48	32.2	26.8	1631
229	1050	-317	170	12	48	38.79	-5 47	4.8	26.5	1061
232	1047	-243	50	12	48	38.57	-5 47	32.8	26.1	1260
233	1052	-247	66	12	48	38.53	-5 47	29.6	26.4	1268
234	1053	-250	160	12	48	38.04	-5 47	12.2	26.8	1062
235	1054	-228	165	12	48	37.74	-5 47	13.1	27.2	974
236	1055	-177	173	12	48	37.08	-5 47	16.1	27.5	1167
237	1116	-140	210	12	48	36.42	-5 47	12.4	27.1	1169
239	1056	-164	118	12	48	37.22	-5 47	27.1	27.1	1174
240	1057	-170	108	12	48	37.35	-5 47	28.3	27.0	1185
241	1058	-186	123	12	48	37.47	-5 47	24.2	27.0	1293
242	1059	-186	116	12	48	37.51	-5 47	25.6	26.3	1159
243	1060	-215	101	12	48	37.95	-5 47	25.8	26.5	1253
245	1061	-214	55	12	48	38.19	-5 47	34.3	27.3	1248
246	1048	-183	51	12	48	37.85	-5 47	37.6	25.7	1506
248	1062	-177	65	12	48	37.69	-5 47	35.6	26.9	1418
249	1063	-163	60	12	48	37.54	-5 47	37.5	26.6	1107
250	1064	-154	58	12	48	37.44	-5 47	38.8	27.1	1336
251	1113	-141	40	12	48	37.39	-5 47	43.2	26.2	1246
252	1114	-96	49	12	48	36.79	-5 47	45.3	26.0	930
253	1115	-84	45	12	48	36.67	-5 47	47.1	26.3	1483
254	1117	-79	61	12	48	36.53	-5 47	44.6	26.1	1289
255	1118	-67	56	12	48	36.40	-5 47	46.6	26.3	1195
256	1119	-70	68	12	48	36.36	-5 47	44.0	26.9	1618
257	1120	-71	72	12	48	36.36	-5 47	43.3	26.1	1322
258	1121	-43	60	12	48	36.10	-5 47	47.7	26.6	1357
259	1122	-46	91	12	48	35.95	-5 47	41.8	26.8	1425
260	1123	-26	101	12	48	35.65	-5 47	41.8	26.5	1467
261	1124	-13	88	12	48	35.56	-5 47	45.3	26.5	1334
262	1125	-4	68	12	48	35.57	-5 47	49.9	26.0	1040
263	1126	4	83	12	48	35.39	-5 47	47.7	26.5	1096
264	1127	21	100	12	48	35.09	-5 47	45.9	26.0	1338
265	1128	34	65	12	48	35.12	-5 47	53.3	26.9	1185
266	1190	59	96	12	48	34.65	-5 47	49.8	27.0	1057
268	1192	66	148	12	48	34.27	-5 47	41.1	26.3	1128
269	1129	-59	144	12	48	35.81	-5 47	31.2	26.3	1087
270	1130	-122	154	12	48	36.51	-5 47	24.0	26.0	1091
271	1131	-110	151	12	48	36.38	-5 47	25.6	26.7	1276
272	1132	-80	171	12	48	35.90	-5 47	24.7	25.5	1252

Table 1—Continued

Id, E	Id, W	x , G	y , G	α	(2000)	δ	(2000)	$m(5007)$	Helioc. RV	
273	1133	-84	181	12	48	35.91	-5 47	22.4	26.4	1052
274	1134	-37	226	12	48	35.08	-5 47	18.1	27.5	1145
275	1135	-20	213	12	48	34.94	-5 47	22.2	26.8	1488
276	1136	9	219	12	48	34.55	-5 47	23.4	26.7	1405
374	1137	-120	174	12	48	36.37	-5 47	20.6	27.3	1203
277	1193	95	225	12	48	33.46	-5 47	29.7	27.0	1484
283	1199	99	112	12	48	34.07	-5 47	50.5	26.6	1074
284	1200	89	97	12	48	34.27	-5 47	52.4	26.2	1019
285	1201	92	79	12	48	34.33	-5 47	55.8	26.1	1398
286	1202	95	59	12	48	34.42	-5 47	59.7	26.8	1394
287	1189	82	39	12	48	34.69	-5 48	2.1	26.4	1506
306	1066	-268	299	12	48	37.46	-5 46	45.5	26.9	1119
308	1065	-210	240	12	48	37.10	-5 47	1.2	25.8	1518
309	1068	-164	262	12	48	36.41	-5 47	1.0	26.1	1069
310	1139	-147	288	12	48	36.06	-5 46	57.7	26.6	1205
311	1140	-140	294	12	48	35.93	-5 46	57.3	26.2	1469
312	1141	-129	317	12	48	35.67	-5 46	54.0	26.2	1132
318	1142	-115	255	12	48	35.86	-5 47	6.3	26.8	963
320	1143	-81	313	12	48	35.11	-5 46	58.8	28.0	1522
326	1144	-4	285	12	48	34.33	-5 47	10.5	27.2	1361
327	1145	16	255	12	48	34.26	-5 47	17.5	26.6	1234
328	1210	70	255	12	48	33.61	-5 47	22.0	26.8	1420
350	1146	-78	508	12	48	33.97	-5 46	23.9	27.7	1232
351	1147	41	602	12	48	31.99	-5 46	16.8	26.4	1216
352	1148	7	484	12	48	33.07	-5 46	35.4	27.6	1297
364	1069	-172	705	12	48	33.99	-5 45	40.2	26.9	1472
365	1149	-116	722	12	48	33.21	-5 45	41.8	26.3	1362
366	1150	-32	747	12	48	32.05	-5 45	44.4	26.0	1008
367	1215	101	774	12	48	30.28	-5 45	50.8	27.1	1280
372	1151	-1	900	12	48	30.80	-5 45	19.2	26.5	943
1	-1	-1468	-898	12	48	58.85	-5 48	40.7	26.5	1380
2	-1	-1275	-836	12	48	56.15	-5 48	45.8	26.6	1095
3	-1	-1076	-786	12	48	53.45	-5 48	53.5	27.8	1303
4	-1	-1005	-972	12	48	53.64	-5 49	33.4	-1.0	1128
5	-1	-647	-816	12	48	48.40	-5 49	35.3	26.9	1203
6	-1	-410	-901	12	48	46.00	-5 50	10.9	27.2	975
8	-1	-104	-973	12	48	42.69	-5 50	49.8	-1.0	1191
11	-1	-1302	-659	12	48	55.47	-5 48	11.4	27.4	1192
12	-1	-859	-666	12	48	50.13	-5 48	50.2	27.3	1400
13	-1	-666	-613	12	48	47.49	-5 48	56.9	27.0	1220
14	-1	-613	-700	12	48	47.34	-5 49	17.1	27.5	1025
15	-1	-551	-560	12	48	45.79	-5 48	57.2	26.5	1249
16	-1	-505	-599	12	48	45.45	-5 49	8.0	28.2	1322
17	-1	-471	-745	12	48	45.87	-5 49	37.4	27.1	1278
18	-1	-364	-639	12	48	43.96	-5 49	27.3	26.2	1276
19	-1	-413	-752	12	48	45.20	-5 49	43.5	28.6	1413
27	-1	-1325	-548	12	48	55.12	-5 47	49.3	27.7	1144
28	-1	-987	-405	12	48	50.20	-5 47	52.1	26.6	1381
29	-1	-872	-506	12	48	49.38	-5 48	20.1	27.3	1241
30	-1	-844	-544	12	48	49.25	-5 48	29.5	27.4	1065
31	-1	-829	-533	12	48	49.01	-5 48	28.7	26.4	1183
32	-1	-807	-542	12	48	48.79	-5 48	32.1	27.3	1335
33	-1	-829	-382	12	48	48.16	-5 48	1.4	28.4	1126
34	-1	-782	-446	12	48	47.94	-5 48	17.0	27.3	1290
35	-1	-772	-475	12	48	47.98	-5 48	23.0	27.0	1275
36	-1	-720	-399	12	48	46.92	-5 48	13.7	25.7	1193
37	-1	-685	-435	12	48	46.70	-5 48	23.1	27.5	1225
38	-1	-652	-437	12	48	46.31	-5 48	26.2	27.4	1397
39	-1	-596	-409	12	48	45.48	-5 48	26.0	27.8	1057
40	-1	-565	-426	12	48	45.19	-5 48	31.6	27.4	1038
41	-1	-657	-533	12	48	46.92	-5 48	43.2	26.2	1022
42	-1	-632	-531	12	48	46.60	-5 48	45.1	27.2	1369
44	-1	-400	-490	12	48	43.55	-5 48	57.3	26.9	1269
52	1077	-28	-427	12	48	38.67	-5 49	17.4	27.9	1342
65	-1	-1287	-191	12	48	52.63	-5 46	48.0	26.4	1246
66	-1	-1255	-266	12	48	52.67	-5 47	4.3	26.3	1184
67	-1	-1216	-260	12	48	52.15	-5 47	6.5	26.8	1212

Table 1—Continued

Id, E	Id, W	x, G	y, G		α	(2000)	δ	(2000)	$m(5007)$	Helioc. RV
68	-1	-1209	-238	12	48	51.95	-5 47	3.1	27.4	1131
69	-1	-1081	-165	12	48	49.98	-5 47	0.8	26.6	1220
70	-1	-1039	-170	12	48	49.50	-5 47	5.2	27.3	1195
71	-1	-890	-321	12	48	48.55	-5 47	45.1	27.7	1156
72	-1	-760	-177	12	48	46.15	-5 47	30.0	28.0	1469
73	-1	-748	-191	12	48	46.08	-5 47	33.7	27.4	1158
74	-1	-684	-195	12	48	45.33	-5 47	39.8	27.1	1174
75	-1	-630	-214	12	48	44.78	-5 47	47.8	27.9	1461
76	-1	-555	-216	12	48	43.88	-5 47	54.4	27.6	1159
77	-1	-677	-361	12	48	46.19	-5 48	10.4	27.2	1362
78	-1	-589	-345	12	48	45.03	-5 48	15.1	27.0	1324
79	-1	-515	-186	12	48	43.23	-5 47	52.4	27.2	1095
80	-1	-486	-166	12	48	42.75	-5 47	51.2	26.5	1432
81	-1	-398	-211	12	48	41.95	-5 48	6.9	27.4	1090
82	-1	-383	-232	12	48	41.88	-5 48	11.9	26.6	1016
83	-1	-443	-285	12	48	42.91	-5 48	16.5	27.2	1196
84	-1	-497	-332	12	48	43.83	-5 48	20.4	26.5	1274
85	-1	-412	-326	12	48	42.77	-5 48	26.6	27.6	1125
114	-1	-1513	-139	12	48	55.08	-5 46	19.5	27.2	1378
115	-1	-1235	26	12	48	50.76	-5 46	13.1	27.2	1336
116	-1	-1111	31	12	48	49.24	-5 46	22.7	26.5	1379
117	-1	-1021	-15	12	48	48.40	-5 46	38.6	28.0	1302
118	-1	-1003	-64	12	48	48.46	-5 46	49.0	26.9	1418
119	-1	-854	36	12	48	46.08	-5 46	43.6	25.9	1353
120	-1	-856	-91	12	48	46.83	-5 47	6.3	27.5	1310
121	-1	-889	-149	12	48	47.56	-5 47	14.1	27.0	1448
122	-1	-816	-133	12	48	46.58	-5 47	17.4	27.5	1165
123	-1	-721	13	12	48	44.60	-5 46	59.0	27.3	1258
124	-1	-648	12	12	48	43.71	-5 47	5.2	27.2	1080
125	-1	-636	8	12	48	43.59	-5 47	7.1	26.5	1479
126	-1	-616	32	12	48	43.21	-5 47	4.5	27.0	1037
127	-1	-600	22	12	48	43.08	-5 47	7.6	27.6	1212
128	-1	-710	-44	12	48	44.78	-5 47	10.2	27.3	1087
129	-1	-618	-55	12	48	43.73	-5 47	19.9	27.4	1326
130	-1	-534	-65	12	48	42.77	-5 47	28.9	26.0	1528
131	-1	-552	-90	12	48	43.13	-5 47	32.0	27.3	1196
132	-1	-562	-115	12	48	43.40	-5 47	35.6	27.0	1237
133	-1	-519	3	12	48	42.19	-5 47	17.9	27.9	1152
134	-1	-441	-7	12	48	41.31	-5 47	26.3	27.3	1116
135	-1	-339	-0	12	48	40.03	-5 47	33.8	27.4	1089
137	-1	-447	-53	12	48	41.64	-5 47	34.2	27.4	1041
138	-1	-396	-66	12	48	41.09	-5 47	40.9	26.8	1448
139	-1	-429	-112	12	48	41.76	-5 47	46.2	27.7	1143
140	-1	-416	-110	12	48	41.59	-5 47	47.1	26.4	1034
141	-1	-425	-122	12	48	41.76	-5 47	48.5	27.0	1489
142	-1	-473	-141	12	48	42.46	-5 47	47.9	26.3	1421
152	1033	-193	13	12	48	38.18	-5 47	43.7	27.0	1044
154	1035	-193	1	12	48	38.25	-5 47	45.8	26.9	1171
187	1168	107	19	12	48	34.49	-5 48	7.9	26.8	1308
210	-1	-1412	230	12	48	51.76	-5 45	21.2	27.8	1267
211	-1	-1255	79	12	48	50.71	-5 46	1.8	25.8	1262
212	-1	-1077	60	12	48	48.66	-5 46	20.3	26.8	1081
213	-1	-1024	93	12	48	47.82	-5 46	18.9	-1.0	1367
214	-1	-1002	87	12	48	47.59	-5 46	21.9	-1.0	1065
215	-1	-653	228	12	48	42.55	-5 46	25.8	27.7	1312
216	-1	-644	129	12	48	42.99	-5 46	44.4	26.4	1367
217	-1	-623	138	12	48	42.69	-5 46	44.6	26.3	1198
218	-1	-585	88	12	48	42.51	-5 46	56.8	27.6	1331
219	-1	-522	157	12	48	41.35	-5 46	49.7	26.6	1450
220	-1	-457	224	12	48	40.19	-5 46	43.2	27.4	1131
221	-1	-470	98	12	48	41.06	-5 47	4.8	27.0	1388
222	-1	-430	144	12	48	40.32	-5 46	59.9	26.8	1394
223	-1	-393	176	12	48	39.69	-5 46	57.2	27.7	1328
224	-1	-415	87	12	48	40.46	-5 47	11.4	27.1	1257
225	-1	-378	127	12	48	39.78	-5 47	7.5	27.2	1207
226	-1	-370	120	12	48	39.72	-5 47	9.3	26.7	1015
227	-1	-362	97	12	48	39.76	-5 47	14.1	27.5	1324

Table 1—Continued

Id, E	Id, W	x, G	y, G		α	(2000)	δ	(2000)	$m(5007)$	Helioc. RV
228	-1	-349	161	12	48	39.23	-5 47	3.7	27.2	1294
231	1051	-272	53	12	48	38.92	-5 47	29.9	28.0	1272
238	-1	-154	134	12	48	37.03	-5 47	25.1	27.8	1002
244	-1	-199	87	12	48	37.83	-5 47	29.7	27.8	1322
247	1049	-183	24	12	48	37.99	-5 47	42.5	26.4	1408
267	1191	67	94	12	48	34.56	-5 47	51.1	27.1	1574
290	1205	135	100	12	48	33.70	-5 47	55.7	27.1	1419
293	-1	-1016	390	12	48	46.05	-5 45	25.8	27.9	1160
294	-1	-955	420	12	48	45.13	-5 45	25.4	28.2	1188
295	-1	-835	316	12	48	44.26	-5 45	54.5	26.5	1522
296	-1	-742	404	12	48	42.63	-5 45	46.4	27.5	1208
297	-1	-739	275	12	48	43.32	-5 46	10.1	27.8	1375
298	-1	-556	323	12	48	40.83	-5 46	16.8	26.7	1123
299	-1	-662	319	12	48	42.14	-5 46	8.6	27.7	1367
300	-1	-441	356	12	48	39.25	-5 46	20.5	26.6	1321
301	-1	-447	252	12	48	39.91	-5 46	38.8	26.7	1260
302	-1	-387	374	12	48	38.49	-5 46	21.9	28.0	1159
303	-1	-300	387	12	48	37.35	-5 46	26.8	27.2	1247
304	-1	-310	337	12	48	37.76	-5 46	35.2	27.2	1263
305	-1	-250	382	12	48	36.78	-5 46	32.1	27.9	1111
307	1067	-275	290	12	48	37.61	-5 46	46.5	27.7	1379
313	-1	-175	353	12	48	36.03	-5 46	43.7	27.1	1549
314	-1	-176	363	12	48	35.99	-5 46	41.7	26.3	1172
315	-1	-169	404	12	48	35.67	-5 46	35.0	26.3	1490
316	-1	-134	392	12	48	35.31	-5 46	40.1	26.9	1479
317	-1	-129	387	12	48	35.27	-5 46	41.3	27.3	1181
319	-1	-105	316	12	48	35.39	-5 46	56.1	27.8	1489
321	-1	-109	328	12	48	35.37	-5 46	53.8	27.9	1251
322	-1	-98	352	12	48	35.10	-5 46	50.3	26.4	1285
323	-1	-58	356	12	48	34.58	-5 46	52.9	28.3	1372
324	-1	-33	359	12	48	34.27	-5 46	54.5	27.7	1151
325	-1	-52	434	12	48	34.08	-5 46	39.3	26.5	1150
329	-1	99	368	12	48	32.62	-5 47	4.1	26.9	1246
330	-1	100	347	12	48	32.72	-5 47	8.0	27.5	1200
335	-1	-1471	535	12	48	50.74	-5 44	21.0	26.4	1134
336	-1	-1449	556	12	48	50.36	-5 44	19.0	27.0	1156
337	-1	-830	625	12	48	42.44	-5 44	58.8	27.8	1343
339	-1	-776	498	12	48	42.51	-5 45	26.5	27.1	1355
340	-1	-729	510	12	48	41.87	-5 45	28.2	27.7	1361
341	-1	-751	468	12	48	42.37	-5 45	34.0	27.5	1379
342	-1	-684	597	12	48	40.83	-5 45	16.3	27.1	1365
343	-1	-646	632	12	48	40.17	-5 45	13.2	26.2	1353
344	-1	-641	547	12	48	40.59	-5 45	29.0	28.0	1107
345	-1	-562	515	12	48	39.81	-5 45	41.5	27.6	1129
346	-1	-566	481	12	48	40.06	-5 45	47.4	27.0	985
347	-1	-519	608	12	48	38.76	-5 45	28.3	27.7	1404
348	-1	-346	485	12	48	37.35	-5 46	5.2	26.4	1165
349	-1	-185	445	12	48	35.63	-5 46	26.1	27.7	1407
353	-1	13	446	12	48	33.21	-5 46	42.7	27.9	1298
354	-1	43	455	12	48	32.80	-5 46	43.6	27.8	1437
357	-1	-1361	805	12	48	47.87	-5 43	41.4	27.2	1310
358	-1	-649	812	12	48	39.18	-5 44	40.4	26.0	1099
359	-1	-646	820	12	48	39.09	-5 44	39.1	27.2	1150
360	-1	-548	810	12	48	37.96	-5 44	49.2	27.3	1353
361	-1	-532	788	12	48	37.89	-5 44	54.6	26.6	1315
362	-1	-584	642	12	48	39.36	-5 45	16.7	26.5	1182
363	-1	-392	802	12	48	36.12	-5 45	3.9	27.6	1332
369	-1	-498	943	12	48	36.61	-5 44	29.4	27.7	1137
370	-1	-382	960	12	48	35.10	-5 44	36.2	27.8	1178
371	-1	-355	1014	12	48	34.46	-5 44	28.6	27.6	1459
230	1046	-277	38	12	48	39.04	-5 47	32.0	27.0	1010
10	1152	198	-913	12	48	38.66	-5 51	4.5	27.3	1369
26	1153	138	-669	12	48	38.01	-5 50	15.2	27.2	1133
58	1154	131	-410	12	48	36.64	-5 49	27.7	27.4	1364
59	1155	176	-402	12	48	36.05	-5 49	30.2	27.1	1363
60	1156	204	-410	12	48	35.75	-5 49	33.8	27.0	1251
63	1159	158	-497	12	48	36.79	-5 49	45.7	27.5	1187

Table 1—Continued

Id, E	Id, W	x , G	y , G		α	(2000)	δ	(2000)	$m(5007)$	Helioc. RV
64	1160	191	-523	12	48	36.54	-5 49	53.3	26.7	1118
113	1161	121	-367	12	48	36.52	-5 49	18.9	27.8	1339
207	1164	130	-149	12	48	35.18	-5 48	40.3	27.2	1516
188	1169	145	23	12	48	34.02	-5 48	10.5	26.6	1058
189	1170	146	17	12	48	34.04	-5 48	11.7	26.7	1321
190	1171	156	27	12	48	33.86	-5 48	10.8	26.9	1356
191	1172	168	34	12	48	33.68	-5 48	10.4	26.1	1336
192	1173	185	25	12	48	33.53	-5 48	13.4	26.6	1525
194	1174	175	1	12	48	33.78	-5 48	17.0	26.7	1485
195	1175	209	-5	12	48	33.40	-5 48	21.0	26.7	1419
196	1176	120	-10	12	48	34.51	-5 48	14.3	27.0	880
197	1177	145	-13	12	48	34.21	-5 48	16.9	26.0	936
198	1178	138	-27	12	48	34.39	-5 48	18.9	25.7	1269
199	1179	156	-37	12	48	34.22	-5 48	22.2	26.5	1352
201	1181	203	-57	12	48	33.76	-5 48	29.6	27.0	1160
202	1182	191	-73	12	48	34.00	-5 48	31.7	26.1	1348
206	1186	146	-116	12	48	34.79	-5 48	35.7	25.6	1424
208	1187	153	-144	12	48	34.86	-5 48	41.3	26.9	1318
209	1188	174	-143	12	48	34.60	-5 48	43.1	27.0	1415
279	1195	191	183	12	48	32.54	-5 47	45.4	27.3	1277
280	1196	160	161	12	48	33.04	-5 47	46.8	27.6	1284
281	1197	137	149	12	48	33.40	-5 47	46.9	26.4	1422
282	1198	127	129	12	48	33.62	-5 47	49.7	27.5	1343
288	1203	126	74	12	48	33.96	-5 47	59.6	26.9	984
289	1204	136	79	12	48	33.81	-5 47	59.7	26.4	1121
291	1206	180	100	12	48	33.16	-5 47	59.5	26.8	1333
292	1207	183	53	12	48	33.38	-5 48	8.2	26.8	1384
331	1208	125	250	12	48	32.96	-5 47	27.6	27.5	1351
332	1209	154	247	12	48	32.63	-5 47	30.7	25.9	1564
333	1211	191	263	12	48	32.10	-5 47	30.8	27.0	1349
334	1212	155	284	12	48	32.41	-5 47	24.0	27.2	1265
355	1213	194	515	12	48	30.62	-5 46	45.6	27.7	1089
356	1214	198	482	12	48	30.76	-5 46	51.7	26.8	1220
368	1216	183	784	12	48	29.22	-5 45	55.7	25.9	1337
373	1217	162	1021	12	48	28.12	-5 45	11.1	27.3	1229
-1	1501	15	149	12	48	34.88	-5 47	36.5	27.5	1066
-1	1502	-81	587	12	48	33.57	-5 46	9.0	27.6	1267
-1	1503	210	-945	12	48	38.72	-5 51	11.2	27.4	1291
-1	1504	235	-611	12	48	36.53	-5 50	12.9	27.7	1395
-1	1505	223	-437	12	48	35.68	-5 49	40.4	27.4	1503
-1	1506	218	-281	12	48	34.85	-5 49	11.7	26.8	1424
-1	1507	194	-263	12	48	35.04	-5 49	6.3	27.5	1403
-1	1508	211	-183	12	48	34.38	-5 48	53.2	27.7	1244
-1	1509	158	-13	12	48	34.06	-5 48	18.0	27.4	1326
-1	1510	227	-6	12	48	33.18	-5 48	22.6	26.7	1378
-1	1511	241	3	12	48	32.96	-5 48	22.2	25.6	1315
-1	1512	244	-47	12	48	33.21	-5 48	31.5	26.8	1574
-1	1513	241	-79	12	48	33.43	-5 48	37.0	27.2	1142
-1	1514	224	-98	12	48	33.74	-5 48	38.9	27.5	1408
-1	1515	240	-133	12	48	33.75	-5 48	46.8	26.6	1309
-1	1516	172	70	12	48	33.42	-5 48	4.2	27.0	1243
-1	1517	234	79	12	48	32.62	-5 48	7.7	26.6	1551
-1	1518	214	136	12	48	32.53	-5 47	55.7	27.4	1205
-1	1519	218	311	12	48	31.50	-5 47	24.4	27.5	1371
-1	1601	310	-772	12	48	36.53	-5 50	48.4	27.6	1314
-1	1602	403	-872	12	48	35.96	-5 51	14.4	26.1	1274
-1	1603	268	-619	12	48	36.17	-5 50	17.1	27.6	1104
-1	1604	291	-725	12	48	36.48	-5 50	38.2	27.6	1357
-1	1605	318	-740	12	48	36.24	-5 50	43.3	27.0	1298
-1	1606	349	-743	12	48	35.88	-5 50	46.5	26.9	1243
-1	1607	423	-696	12	48	34.72	-5 50	44.3	26.8	1206
-1	1608	334	-550	12	48	34.97	-5 50	10.3	27.5	1282
-1	1609	323	-506	12	48	34.85	-5 50	1.5	27.2	1460
-1	1610	394	-464	12	48	33.75	-5 49	59.7	27.8	1377
-1	1611	272	-404	12	48	34.90	-5 49	38.5	26.4	1176
-1	1612	248	-360	12	48	34.94	-5 49	28.5	27.7	1531
-1	1613	276	-350	12	48	34.53	-5 49	29.1	27.4	1357

Table 1—Continued

Id, E	Id, W	x , G	y , G	α	(2000)	δ	(2000)	$m(5007)$	Helioc. RV	
-1	1614	314	-364	12	48	34.15	-5 49	34.9	27.4	1208
-1	1615	276	-341	12	48	34.49	-5 49	27.4	27.4	1340
-1	1616	293	-311	12	48	34.12	-5 49	23.5	27.8	1408
-1	1617	388	-325	12	48	33.04	-5 49	34.1	27.5	1376
-1	1618	259	-264	12	48	34.26	-5 49	12.0	27.0	1144
-1	1619	282	-238	12	48	33.83	-5 49	9.2	27.6	1277
-1	1620	358	-262	12	48	33.04	-5 49	20.1	27.9	1188
-1	1621	373	-252	12	48	32.80	-5 49	19.6	27.3	1445
-1	1622	393	-271	12	48	32.66	-5 49	24.7	26.8	1404
-1	1623	427	-252	12	48	32.15	-5 49	24.3	26.1	964
-1	1624	281	-177	12	48	33.49	-5 48	58.1	25.7	1124
-1	1625	395	-156	12	48	31.99	-5 49	4.1	27.0	1152
-1	1626	281	-138	12	48	33.28	-5 48	51.0	26.5	1305
-1	1627	372	-120	12	48	32.07	-5 48	55.7	26.1	1366
-1	1628	348	-62	12	48	32.03	-5 48	43.0	27.4	1298
-1	1629	376	-64	12	48	31.70	-5 48	45.8	27.4	1503
-1	1630	409	-69	12	48	31.33	-5 48	49.5	27.1	1409
-1	1631	445	-46	12	48	30.76	-5 48	48.4	27.5	1431
-1	1632	249	-11	12	48	32.95	-5 48	25.3	27.1	1018
-1	1633	291	4	12	48	32.34	-5 48	26.3	26.8	1512
-1	1634	418	-1	12	48	30.84	-5 48	38.0	28.1	1122
-1	1635	429	-7	12	48	30.74	-5 48	40.1	27.3	1370
-1	1636	374	19	12	48	31.26	-5 48	30.7	25.7	1428
-1	1637	271	28	12	48	32.46	-5 48	20.2	26.0	1322
-1	1638	317	58	12	48	31.73	-5 48	18.7	26.9	1536
-1	1639	283	98	12	48	31.92	-5 48	8.6	26.3	1466
-1	1640	326	117	12	48	31.28	-5 48	8.8	26.4	1639
-1	1641	434	99	12	48	30.07	-5 48	21.2	27.4	1079
-1	1642	428	138	12	48	29.92	-5 48	13.7	27.8	1199
-1	1643	392	152	12	48	30.27	-5 48	8.0	26.6	1152
-1	1644	438	175	12	48	29.60	-5 48	7.8	27.4	1143
-1	1645	303	170	12	48	31.26	-5 47	57.2	26.5	1198
-1	1646	353	192	12	48	30.53	-5 47	57.5	27.3	1128
-1	1647	366	199	12	48	30.32	-5 47	57.3	27.1	1381
-1	1648	343	415	12	48	29.38	-5 47	16.4	25.8	1447
-1	1650	339	463	12	48	29.16	-5 47	7.3	26.1	1198
-1	1651	429	591	12	48	27.34	-5 46	51.7	27.6	1294
-1	1652	441	624	12	48	27.00	-5 46	46.8	27.5	1300
-1	1653	306	473	12	48	29.51	-5 47	2.6	27.5	1344
-1	1654	339	723	12	48	27.68	-5 46	20.1	26.9	1321
-1	1655	433	815	12	48	26.02	-5 46	11.5	27.3	1138
-1	1656	272	864	12	48	27.70	-5 45	49.0	26.6	1469
-1	1657	257	1034	12	48	26.92	-5 45	16.9	27.0	1167
-1	1658	301	964	12	48	26.77	-5 45	33.2	27.4	1252
-1	1659	619	-821	12	48	33.05	-5 51	23.6	27.1	1205
-1	1660	603	-513	12	48	31.49	-5 50	26.5	27.4	1176
-1	1661	630	-389	12	48	30.45	-5 50	6.3	25.8	1252
-1	1662	522	-266	12	48	31.07	-5 49	34.8	27.3	1371
-1	1663	542	-188	12	48	30.40	-5 49	22.5	26.4	1218
-1	1664	460	-131	12	48	31.06	-5 49	5.1	26.8	1367
-1	1665	511	-67	12	48	30.08	-5 48	57.9	27.5	1197
-1	1666	541	-50	12	48	29.61	-5 48	57.3	26.4	1388
-1	1667	629	-105	12	48	28.85	-5 49	14.8	26.7	1542
-1	1668	646	-132	12	48	28.80	-5 49	21.1	26.2	1453
-1	1669	615	-20	12	48	28.55	-5 48	58.2	27.5	1140
-1	1670	627	-12	12	48	28.36	-5 48	57.8	27.4	1327
-1	1671	562	13	12	48	29.01	-5 48	47.8	26.0	1293
-1	1672	475	5	12	48	30.10	-5 48	41.8	27.5	1381
-1	1673	547	42	12	48	29.02	-5 48	41.2	27.0	1172
-1	1674	601	0	12	48	28.60	-5 48	53.4	27.7	1237
-1	1675	504	65	12	48	29.42	-5 48	33.4	27.5	1500
-1	1676	519	84	12	48	29.13	-5 48	31.1	26.6	1337
-1	1677	608	159	12	48	27.61	-5 48	25.2	26.8	1286
-1	1678	478	208	12	48	28.92	-5 48	5.1	26.6	1319
-1	1679	498	213	12	48	28.65	-5 48	6.1	26.6	1327
-1	1680	491	252	12	48	28.51	-5 47	58.4	27.4	1180
-1	1681	477	266	12	48	28.60	-5 47	54.7	26.2	1071

Table 1—Continued

Id, E	Id, W	x , G	y , G	α	(2000)	δ	(2000)	$m(5007)$	Helioc. RV	
-1	1682	547	293	12	48	27.59	-5 47	55.7	26.4	1228
-1	1683	585	294	12	48	27.12	-5 47	58.8	25.6	1097
-1	1684	469	351	12	48	28.21	-5 47	38.7	26.6	1399
-1	1685	499	375	12	48	27.71	-5 47	36.8	27.3	1272
-1	1686	626	363	12	48	26.24	-5 47	49.8	26.8	1364
-1	1687	495	410	12	48	27.57	-5 47	30.2	26.5	1314
-1	1688	549	428	12	48	26.80	-5 47	31.5	27.9	1114
-1	1689	602	421	12	48	26.20	-5 47	37.2	27.8	1711
-1	1690	474	475	12	48	27.46	-5 47	16.5	27.1	1563
-1	1691	489	479	12	48	27.25	-5 47	17.1	26.6	1335
-1	1692	573	578	12	48	25.66	-5 47	6.5	26.2	1340
-1	1693	528	638	12	48	25.87	-5 46	51.8	-1.0	1263
-1	1694	518	589	12	48	26.27	-5 46	59.6	27.8	1185
-1	1695	596	910	12	48	23.50	-5 46	8.2	26.5	1270
-1	1696	624	1057	12	48	22.32	-5 45	43.9	27.3	1072
-1	1697	748	-706	12	48	30.83	-5 51	13.8	27.7	1235
-1	1698	703	-625	12	48	30.92	-5 50	55.3	26.9	1311
-1	1699	719	-630	12	48	30.75	-5 50	57.6	27.8	1460
-1	1700	826	-597	12	48	29.26	-5 51	0.8	26.5	1297
-1	1701	736	-420	12	48	29.35	-5 50	20.9	26.7	1332
-1	1702	666	-386	12	48	30.01	-5 50	8.9	26.8	1259
-1	1703	703	-324	12	48	29.19	-5 50	0.8	26.1	1124
-1	1704	719	-294	12	48	28.83	-5 49	56.7	27.4	1144
-1	1705	818	-148	12	48	26.81	-5 49	38.7	26.8	1393
-1	1706	673	-131	12	48	28.47	-5 49	23.3	27.2	1401
-1	1707	764	-101	12	48	27.20	-5 49	25.6	25.8	1253
-1	1708	747	-63	12	48	27.19	-5 49	17.2	27.6	1237
-1	1709	816	-8	12	48	26.04	-5 49	13.2	26.0	1289
-1	1710	672	10	12	48	27.68	-5 48	57.7	27.1	1477
-1	1711	677	169	12	48	26.71	-5 48	29.3	26.1	1165
-1	1712	663	174	12	48	26.86	-5 48	27.3	26.4	1069
-1	1713	688	214	12	48	26.33	-5 48	22.0	26.1	1084
-1	1714	783	186	12	48	25.33	-5 48	35.3	27.2	1350
-1	1715	824	209	12	48	24.71	-5 48	34.5	26.5	1204
-1	1716	791	334	12	48	24.40	-5 48	9.3	27.8	1358
-1	1717	837	428	12	48	23.31	-5 47	56.0	27.3	1331
-1	1718	744	706	12	48	22.86	-5 46	57.7	27.6	1257
-1	1719	739	1015	12	48	21.17	-5 46	1.3	27.5	1139
-1	1720	916	-925	12	48	30.03	-5 52	7.8	27.5	1200
-1	1721	945	-925	12	48	29.68	-5 52	10.3	27.5	1140
-1	1722	955	-400	12	48	26.58	-5 50	36.1	27.5	1172
-1	1723	1008	-226	12	48	24.93	-5 50	9.0	26.2	1340
-1	1724	1012	80	12	48	23.15	-5 49	14.1	27.3	1130
-1	1725	1029	133	12	48	22.64	-5 49	5.8	27.1	1251
-1	1726	966	160	12	48	23.26	-5 48	55.5	27.5	1358
-1	1727	1032	184	12	48	22.32	-5 48	56.9	26.0	1300
-1	1728	989	339	12	48	21.96	-5 48	25.1	26.3	1380
-1	1729	875	540	12	48	22.21	-5 47	38.9	27.5	1526
-1	1730	969	664	12	48	20.36	-5 47	24.5	27.3	1307
-1	1731	891	934	12	48	19.78	-5 46	29.1	25.9	1203
-1	1732	1099	-687	12	48	26.44	-5 51	40.3	26.0	1288
-1	1733	1170	-458	12	48	24.28	-5 51	5.0	27.1	1417
-1	1734	1179	-400	12	48	23.85	-5 50	55.1	26.3	1206
-1	1735	1052	-226	12	48	24.40	-5 50	12.9	27.2	1345
-1	1736	1117	-190	12	48	23.41	-5 50	11.8	27.2	1457
-1	1737	1074	-139	12	48	23.65	-5 49	59.0	26.0	1338
-1	1738	1201	334	12	48	19.41	-5 48	44.2	26.8	1398
-1	1739	1121	349	12	48	20.31	-5 48	34.6	27.2	1306
-1	1740	1051	398	12	48	20.88	-5 48	19.7	27.3	1148
-1	1741	1073	952	12	48	17.46	-5 46	41.3	26.5	1361
-1	1742	1404	-344	12	48	20.78	-5 51	4.1	26.6	-1
-1	1743	1298	-307	12	48	21.87	-5 50	48.5	26.8	1395
-1	1744	1352	-220	12	48	20.71	-5 50	37.0	26.8	-1
-1	1745	1345	-170	12	48	20.52	-5 50	27.6	26.9	-1
-1	1746	1429	-65	12	48	18.89	-5 50	15.6	26.0	-1
-1	1747	1304	6	12	48	20.02	-5 49	52.4	26.0	1441

^aThe x , G and y , G pixel coordinates have their origin at the center of light of NGC 4697. The x , G coordinate is defined along the major axis of NGC 4697. The units of Right Ascension are hours, minutes and seconds; the units of Declination are degrees, arcminutes, and arcseconds. Heliocentric radial velocities are given in km s^{-1} . In columns 1 & 2 a value of -1 indicates that the object is not present in the corresponding field. In columns 7 & 8 a value of -1 indicates that the corresponding quantity could not be measured.

Table 2. Some additional objects in the field of NGC 4697 ^a

Object	Field	x , G	y , G	α	(2000)	δ	(2000)	Notes	
1	E,W	-136	-278	12	48	39.14	-5 48	41.4	b
2	E,W	-93	239	12	48	35.68	-5 47	11.3	c
3	E,W	190	-449	12	48	36.15	-5 49	40.0	b
4	E,W	32	-270	12	48	37.05	-5 48	54.2	c
5	E,W	96	805	12	48	30.14	-5 45	45.0	b
6	E,W	405	-684	12	48	34.86	-5 50	40.6	c
7	E,W	297	193	12	48	31.20	-5 47	52.8	c
8	E,W	359	115	12	48	30.89	-5 48	12.2	d
9	E,W	159	69	12	48	33.57	-5 48	3.5	d
10	E,W	167	85	12	48	33.39	-5 48	1.3	d
11	E,W	45	117	12	48	34.68	-5 47	45.2	d
12	E,W	152	218	12	48	32.81	-5 47	35.9	f
13	W	564	38	12	48	28.83	-5 48	43.5	e
14	W	584	29	12	48	28.63	-5 48	46.7	e
15	W	807	-656	12	48	29.83	-5 51	9.9	c
16	W	1327	391	12	48	17.54	-5 48	44.3	c
17	W	1044	395	12	48	20.95	-5 48	19.4	b
18	W	391	386	12	48	28.96	-5 47	25.6	f
19	E	-774	630	12	48	41.73	-5 45	2.6	f
20	E	-1510	-412	12	48	56.59	-5 47	9.2	c

^aThe x , G and y , G coordinates have their origin at the center of light of NGC 4697. The x , G coordinate is defined along the major axis of NGC 4697. The units of Right Ascension are hours, minutes and seconds; the units of Declination are degrees, arcminutes, and arcseconds.

^bEmission-line region within an extended source (galaxy).

^cPoint source in onband and grism+onband, visible but not stronger in offband.

^dPoint source in onband, stronger in offband, absent in grism+onband.

^ePoint source in onband, visible but weaker in offband, absent in grism+onband. Variable star?

^fPoint source in onband and grism+onband, not visible in offband, but wrong velocity for NGC 4697 if identified as [O III] $\lambda 5007$.

Fig. 1.— Comparison of old vs. new radial velocity measurements, expressed in hundreds of km s^{-1} , for 367 PNs in the W field. Since there is satisfactory agreement, we have decided to average the two W measurements. See Figs. 2-4.

Fig. 2.— Differences between new W and old W radial velocities as a function of the new W velocities. The velocities are expressed in hundreds of km s^{-1} . The new W velocities are slightly lower, but well within the errors of about 40 km s^{-1} .

Fig. 3.— Differences between new W and old W radial velocities as a function of $m(5007)$. The velocities are expressed in hundreds of km s^{-1} . The new W velocities are slightly lower, but well within the errors of about 40 km s^{-1} . The differences are larger for fainter PNs, as expected, since the quality of the radial velocities depends on the quality of the position measurements.

Fig. 4.— Differences between new W and old E radial velocities as a function of the new W velocities. There are 164 data points. The velocities are expressed in hundreds of km s^{-1} . The new W velocities are slightly lower, but well within the errors of about 40 km s^{-1} .

Fig. 5.— Radial velocities of 531 PNs, in km s^{-1} , as a function of their x -coordinates in arcseconds relative to the center of light of NGC 4697. The x -axis is oriented in the direction of the major axis. This figure replaces Figure 20 in Paper 1.

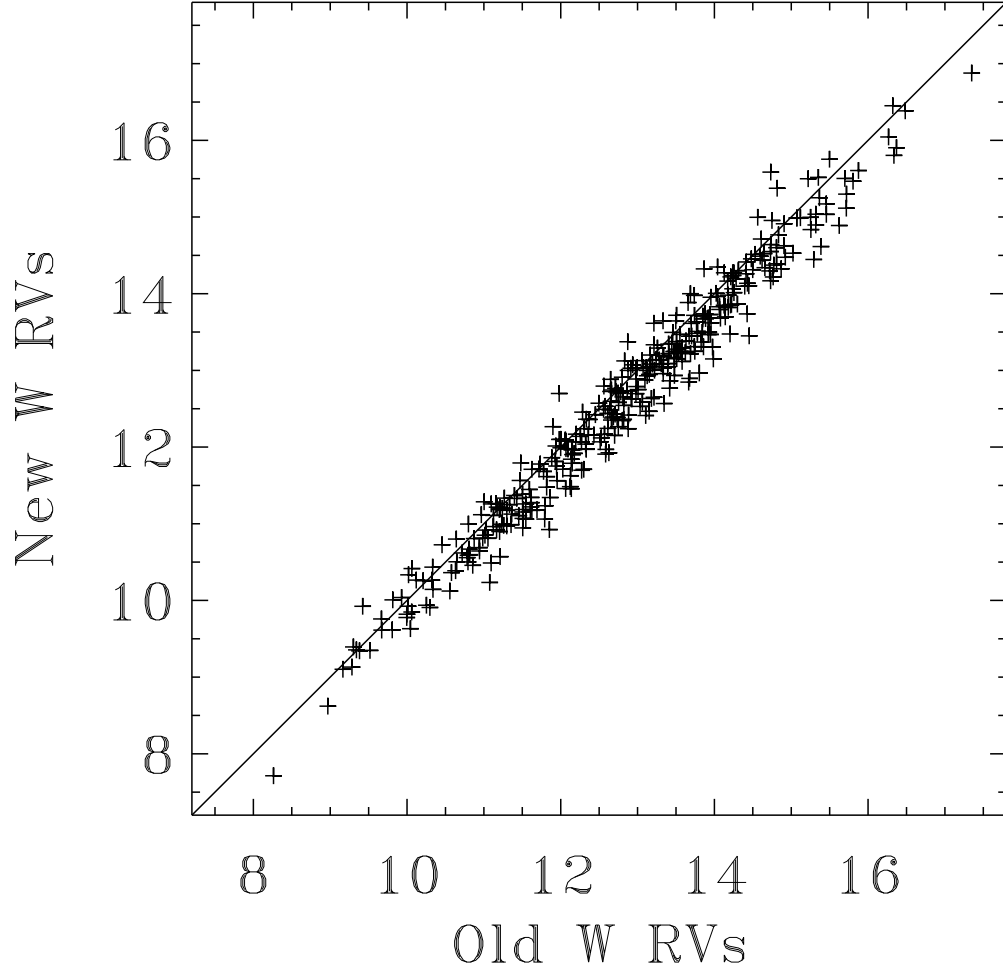


Fig. 1.— Comparison of old vs. new radial velocity measurements, expressed in hundreds of km s^{-1} , for 367 PNs in the W field. Since there is satisfactory agreement, we have decided to average the two W measurements. See Figs. 2-4.

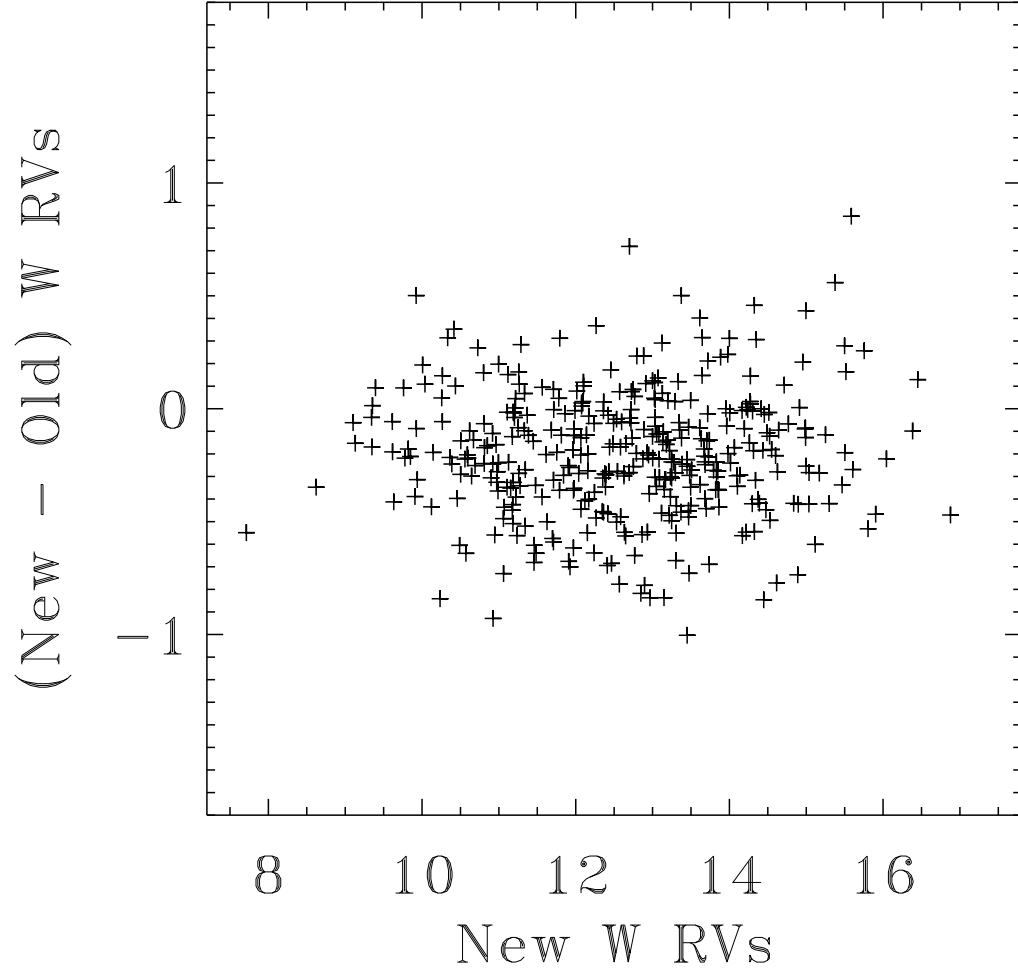


Fig. 2.— Differences between new W and old W radial velocities as a function of the new W velocities. The velocities are expressed in hundreds of km s^{-1} . The new W velocities are slightly lower, but well within the errors of about 40 km s^{-1} .

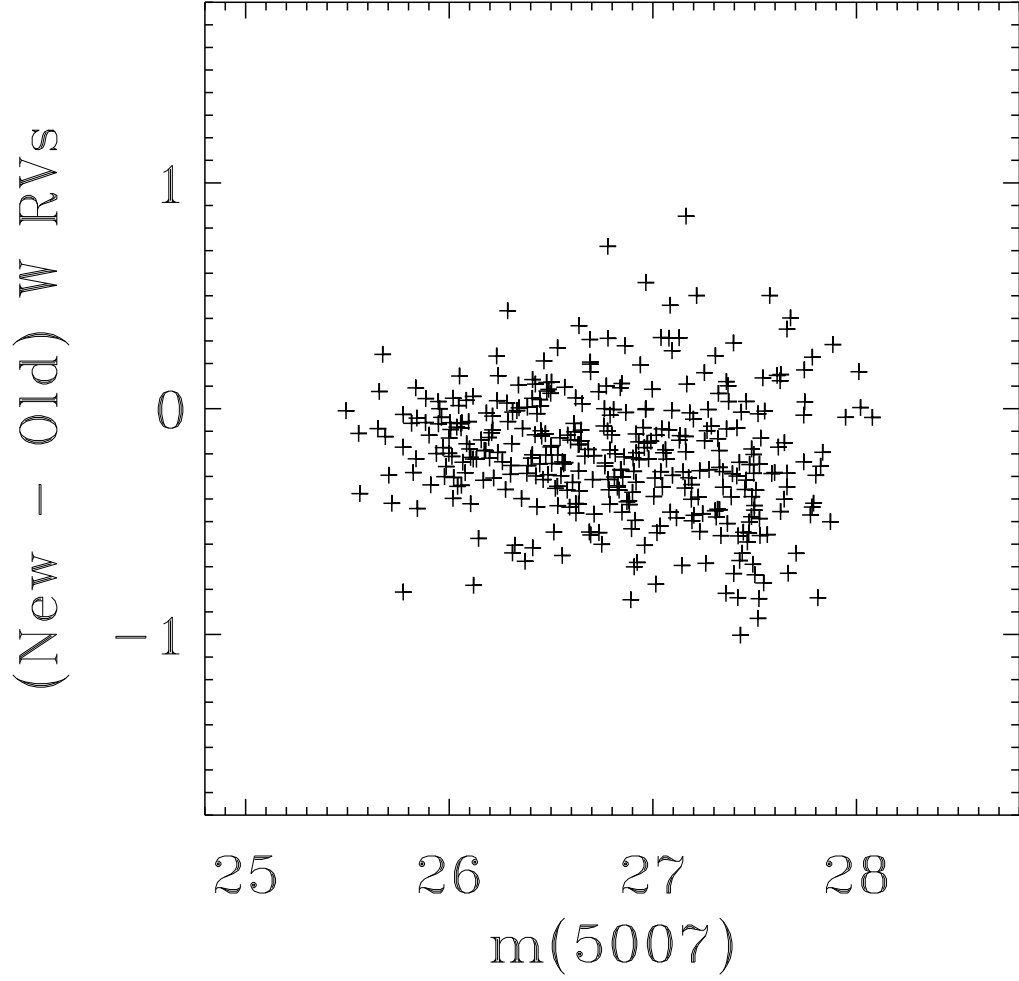


Fig. 3.— Differences between new W and old W radial velocities as a function of $m(5007)$. The velocities are expressed in hundreds of km s^{-1} . The new W velocities are slightly lower, but well within the errors of about 40 km s^{-1} . The differences are larger for fainter PNs, as expected, since the quality of the radial velocities depends on the quality of the position measurements.

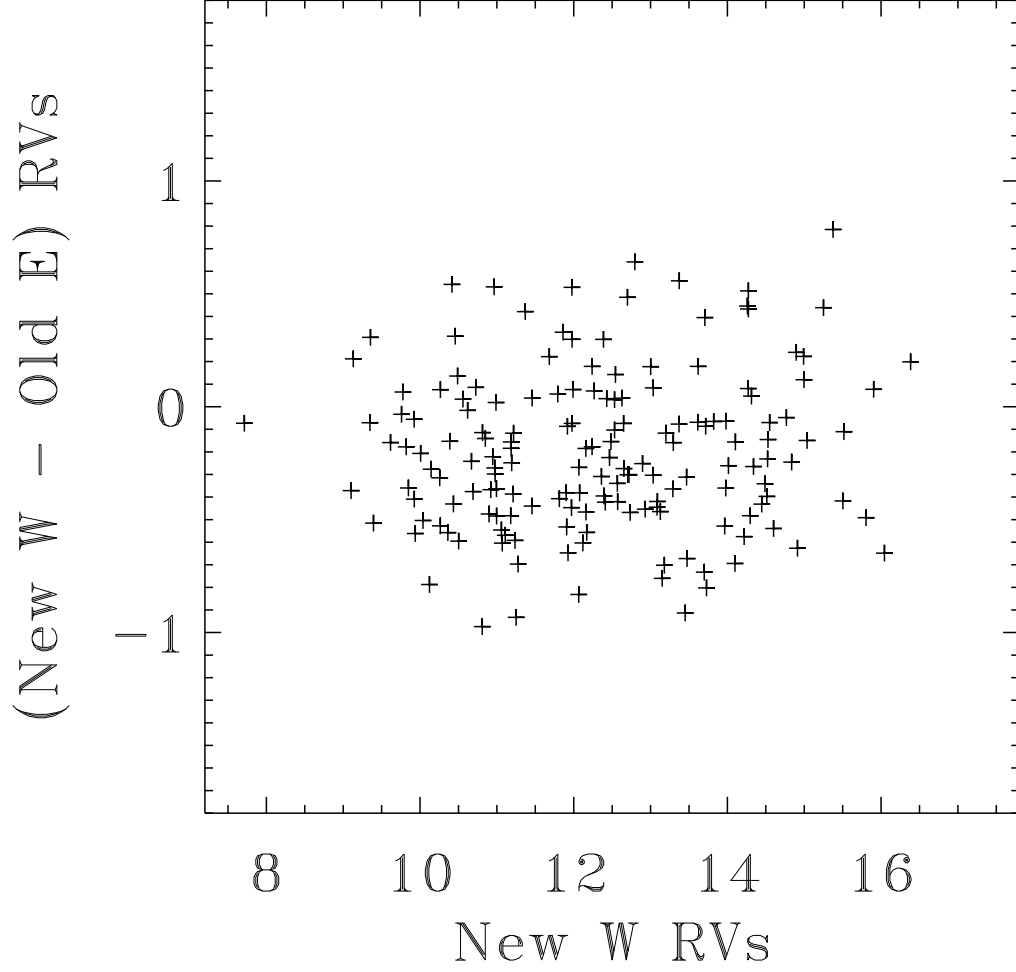


Fig. 4.— Differences between new W and old E radial velocities as a function of the new W velocities. There are 164 data points. The velocities are expressed in hundreds of km s^{-1} . The new W velocities are slightly lower, but well within the errors of about 40 km s^{-1} .

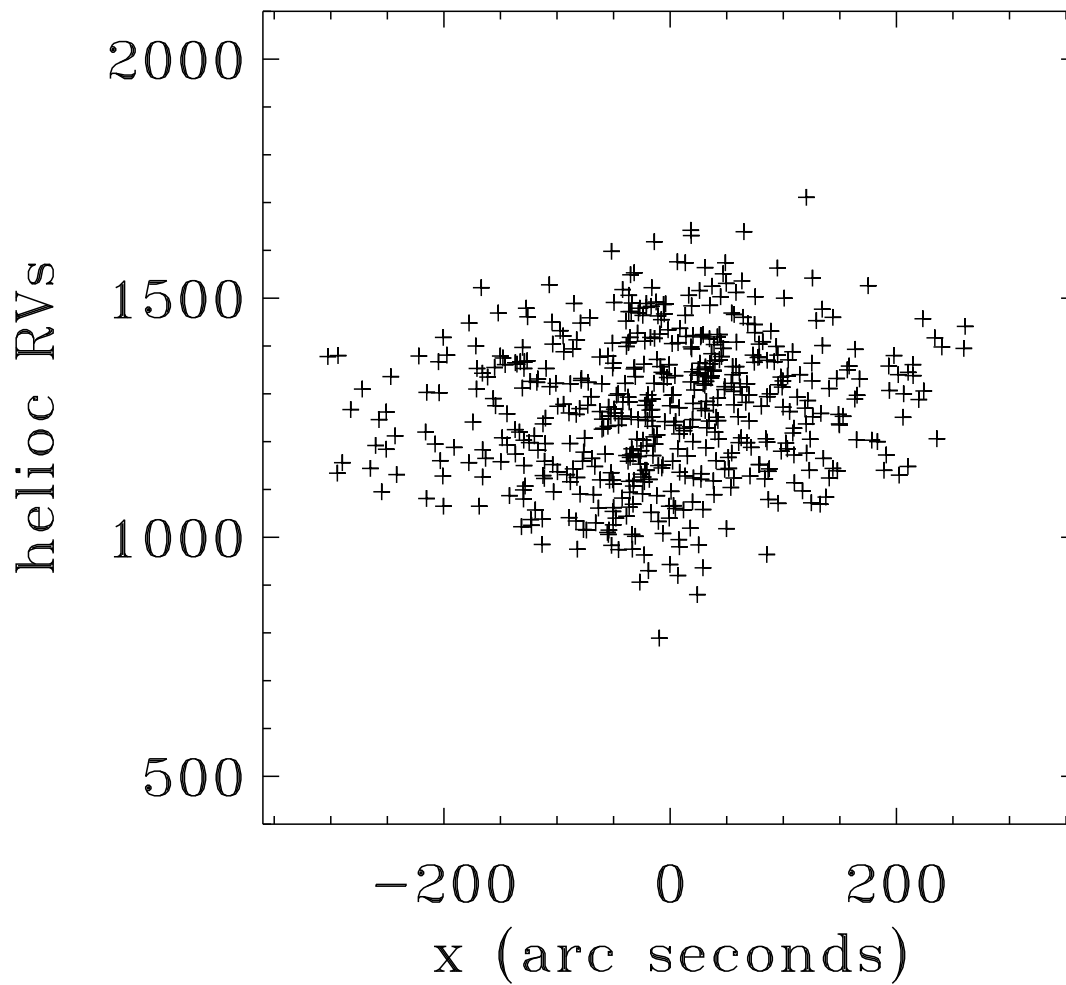


Fig. 5.— Radial velocities of 531 PNs, in km s^{-1} , as a function of their x -coordinates in arcseconds relative to the center of light of NGC 4697. The x -axis is oriented in the direction of the major axis. This figure replaces Figure 20 in Paper 1.